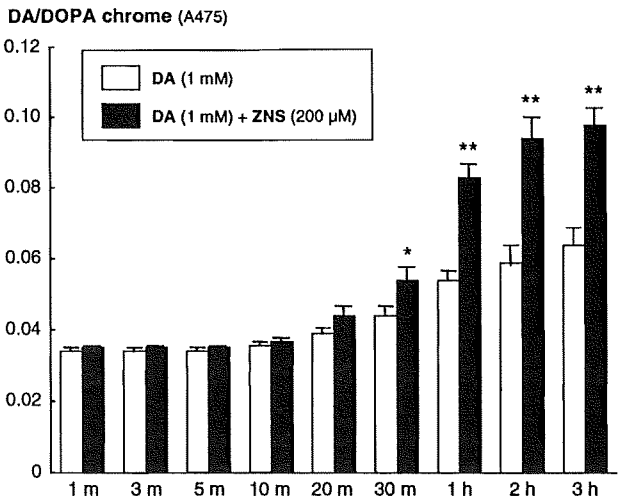

Fig. 3. Effects of ZNS on time-course changes in DA/DOPA chrome generated in a cell-free system. Levels of generated DA/DOPA chrome were measured after incubation of pH-adjusted 1 mM DA (pH 6.8) with/without 200 μM ZNS (pH 6.8) at 37 °C for 1 min to 3 h. Co-incubation of pH-adjusted DA (1 mM) and ZNS (200 μM) at neutral pH significantly increased DA/DOPA chrome at 30 min to 3 h, compared with time-matched pH-adjusted DA alone. Each value is the mean of absorbance at 475 nm ± S.E.M. ($n = 5$). *$p < 0.05$, **$p < 0.001$ compared with time-matched group treated with DA alone.

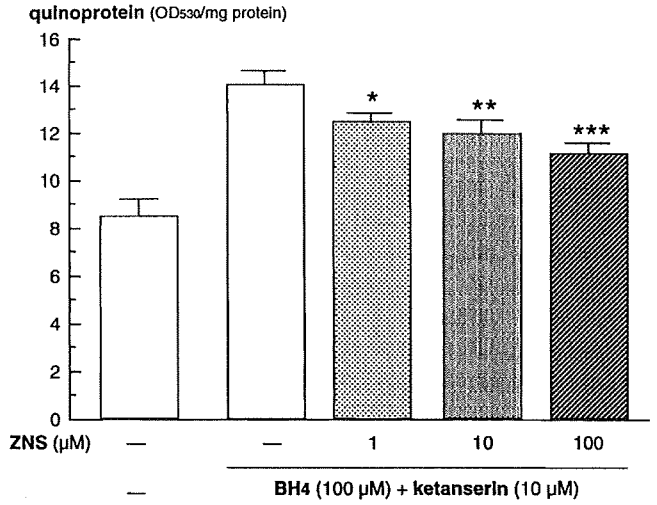

Fig. 5. Effects of ZNS treatment on excess cytosolic free DA-induced quinoprotein formation in dopaminergic CATH.a cells. Quinoprotein level in CATH.a cells were measured after treatment with BH_4 (100 μM) and ketanserin (10 μM), with or without ZNS (1–100 μM) for 3 h. The simultaneous treatment of ZNS (1–100 μM) significantly and dose-dependently inhibited BH_4 plus ketanserin-induced quinoprotein formation. Data are mean ± S.E.M. ($n = 8$). *$p < 0.05$, **$p < 0.01$ and ***$p < 0.001$ compared with cells treated with BH_4 plus ketanserin without ZNS.

chrome level, co-incubation of pH-adjusted 1 mM DA (pH 6.8) and 200 μM ZNS (pH 6.8) at 37 °C significantly increased DA chrome at 30 min to 3 h, compared with time-matched pH-adjusted DA alone.

3.3. *Effects of ZNS on DA quinone formation in CATH.a cells*

We examined changes in DA, its metabolites, quinoprotein and DA/DOPA chrome using *in vitro* dopaminergic CATH.a cells after 5-day treatment of ZNS. Quinoprotein level was significantly decreased after 5-day treatment of ZNS (10–100 μM) (Fig. 4) with reduction of DOPAC level (data not shown). On the other hand, 5-day treatment of ZNS (1–100 μM) significantly increased DA/DOPA chrome level in CATH.a cells (Fig. 4).

Finally, we examined the effects of ZNS on excess cytosolic free DA-induced quinone formation by measuring quinoprotein levels in CATH.a cells after treatment with BH_4 (100 μM) and ketanserin (10 μM) with/without ZNS (1–100 μM) for 3 h. The quinoprotein levels in CATH.a cells co-treated with BH_4 and ketanserin for 3 h (which increase cytosolic free DA) were relatively higher than that in control at day 1 (Fig. 5), in agreement with a previous report (Choi et al., 2005). The simultaneous treatment of ZNS (1–100 μM) significantly and dose-dependently inhibited BH_4- and ketanserin-induced quinoprotein formation in the cells (Fig. 5).

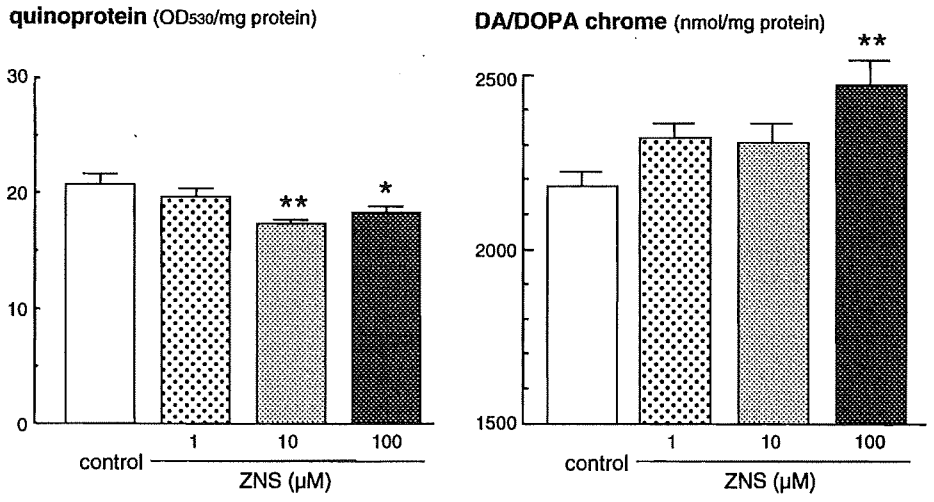

Fig. 4. Effects of long-term treatment of ZNS on quinoprotein and DA/DOPA chrome in dopaminergic CATH.a cells. After treatment with ZNS (1–100 μM) for 5 days, levels of quinoprotein ($n = 5$) and DA/DOPA chrome ($n = 6$) were measured in dopaminergic CATH.a cells, as indicated in Section 2. Data are mean ± S.E.M. *$p < 0.05$, **$p < 0.01$ compared with the control group.

4. Discussion

The main findings of this study are: (1) co-incubation of DA and ZNS in a cell-free system caused conversion of DA to stable melanin via formation of DA-semiquinone radicals and DA chrome; (2) long-term treatment with ZNS for 5 days decreased quinoprotein and increased DA/DOPA chromes in dopaminergic CATH.a cells; and (3) ZNS significantly inhibited quinoprotein formation induced by BH_4 and ketanserin that increase cytosolic free DA in the cells.

Long-term treatment of patients with PD by levodopa frequently causes various adverse effects including the wearing-off phenomenon, dyskinesia and psychiatric symptoms (Ahlskog and Muenter, 2001; Ogawa et al., 2005). However, long-term levodopa treatment-induced adverse effects that might be based on permanent neuronal network remodeling were seen specifically in PD patients but not in normal subjects or neurological diseases other than PD (Ogawa et al., 2005). Since the striatal damaged nerve terminal have too small DA pool to store DA at advanced stage of PD, repeated intermittent pulsatile levodopa stimulation results in free DA excess in the cytosol outside the synaptic vesicle (Sulzer et al., 2000; Sulzer and Zecca, 2000; Asanuma et al., 2003; Ogawa et al., 2005). The previous study revealed that repeated levodopa administration elevated striatal quinoprotein levels specifically on the parkinsonian side, not on the control side, of hemi-parkinsonian mice (Miyazaki et al., 2005). Therefore, the parkinsonian side-specific elevation of quinone generation may be due to excess amount of cytosolic DA outside the synaptic vesicles, which is easily oxidized to DA quinones in damaged dopaminergic nerve terminals after repeated levodopa treatment. In cultured dopaminergic cells, simultaneous treatment with ZNS dose-dependently suppressed BH_4- and ketanserin-induced quinoprotein formation via elevation of cytosolic free DA (Fig. 5), suggesting that ZNS has potent neuroprotective effects against neurotoxicity of DA quinone induced by excess amount of cytosolic DA outside the synaptic vesicles.

The protective effects of ZNS against levodopa-induced DA quinone toxicity in parkinsonian models may be based, in part, on its stabilizing effects against free DA and cytotoxic DA quinone; ZNS can convert free DA to melanin via the formation of DA-semiquinone radicals (Figs. 1 and 2) and subsequent intermediate DA chrome in the cell-free system (Fig. 3). This possible mechanism is also supported by the present results of long-term treatment with ZNS in cultured dopaminergic CATH.a cells. Long-term ZNS treatment in CATH.a cells for 5 days significantly decreased quinoprotein and increased DA/DOPA chromes (Fig. 4) with reduction of DOPAC (data not shown), suggesting that continuous ZNS exposure to DA-rich CATH.a cells promotes conversion of free DA and DA quinone to DA chrome, then to melanin. However, these effects do not seem to be exerted in a dose-dependent manner. Likewise relatively low doses of ZNS (25, 50 mg/day) rather than 100 mg/day significantly improved UPDRS Part III total score in the clinical trial (Murata et al., 2007), there may be optimal concentration range of ZNS to exert its stabilizing effects against DA quinones.

Several neuroprotective strategies have been proposed against DA quinone-induced cytotoxicity: (1) quenching excess free DA and DA quinone, (2) inhibiting quinone formation, and (3) enhancing intrinsic antioxidative system against DA quinone toxicity (Asanuma et al., 2004). Regarding quenching DA quinone, DA quinone can be scavenged by direct conjugation with some drugs, *e.g.*, thiol-containing compounds (*N*-acetylcyteine and dithiothreitol) (Offen et al., 1996) and DA agonists (pergolide and pramipexole) (Asanuma et al., 2005; Miyazaki et al., 2005). Furthermore, another possible method to quench DA quinone-induced cytotoxicity is the conversion of free DA and DA quinone to stable melanin. The final oxidized form of DA quinone, neuromelanin, exerts cytoprotective effects through its binding capacity to toxic metals (Zecca et al., 2003). Although large amount of neuromelanin with iron is reported to be potentially cytotoxic, physiological amount of neuromelanin is not toxic and rather cytoprotective with its high storage capacity for toxic metals in the substantia nigra (Gerlach et al., 2003; Zecca et al., 2003). This cytoprotective potency by stabilization of DA quinone has been clarified by our previous report that melanin-synthesizing enzyme tyrosinase ameliorates methamphetamine-induced neurotoxicity and quinoprotein formation *in vitro* and *in vivo* by its rapid conversion of DA quinone to melanin (Miyazaki et al., 2006). Also in the present study, we showed that ZNS can convert free DA to melanin via the formation of DA quinone and the intermediate DA chrome in the cell-free system. Therefore, these stabilizing effects of ZNS on free DA and DA quinone by the conversion to melanin may be one of the plausible mechanisms of its prevention against DA quinone-induced cytotoxicity.

ZNS is also known to scavenge hydroxyl radicals and nitric oxide radicals in a cell-free system (Mori et al., 1998) and inhibits lipid peroxidation and oxidative DNA damage in the rat brain (Komatsu et al., 2000). The general ROS such as hydroxyl radicals and nitric oxide radicals show widespread toxicity not only in DA neurons but also in other regions. Since the DA quinone is specifically generated from free cytosolic DA (Sulzer et al., 2000), the stabilizing effects of ZNS on free DA and cytotoxic DA quinone as dopaminergic neuron-specific oxidative stress may play a role in its preventing property against DA or levodopa-induced DA quinone toxicity, in addition to its scavenging activity against general ROS.

In conclusion, ZNS suppressed excess cytosolic free DA-induced quinone generation in dopaminergic cells. Furthermore, ZNS stabilized free DA and DA quinone as dopaminergic neuron-specific oxidative stress by the conversion to melanin. The stabilizing effects of ZNS against cytotoxic DA quinones may play a role in the efficacy of its adjunctive treatment to levodopa in parkinsonian patients.

Acknowledgments

This work was supported in part by Health and Labour Sciences Research Grants for Research on Measures for Intractable Diseases, for Research on Psychiatric and Neuro-

logical Diseases and Mental Health, and for Comprehensive Research on Aging and Health from the Japanese Ministry of Health, Labour and Welfare, and by Grants-in-Aid for Young Scientists (B) and for Scientific Research (C) from the Japanese Ministry of Education, Culture, Sports, Science and Technology. We would like to thank Mr. Yusuke Urakubo, Mr. Yasutsugu Tsutsui, and Mr. Masashi Yoshimoto for their technical assistance.

References

Ahlskog, J.E., Muenter, M.D., 2001. Frequency of levodopa-related dyskinesias and motor flucfuations as estimated from the cumulative literature. Mov. Disord. 16, 448–458.

Asanuma, M., Miyazaki, I., Diaz-Corrales, F.J., Ogawa, N., 2004. Quinone formation as dopaminergic neuron-specific oxidative stress in pathogenesis of sporadic Parkinson's disease and neurotoxin-induced parkinsonism. Acta Med. Okayama 58, 221–233.

Asanuma, M., Miyazaki, I., Diaz-Corrales, F.J., Shimizu, M., Tanaka, K., Ogawa, N., 2005. Pramipexole has ameliorating effects on levodopa-induced abnormal dopamine turnover in parkinsonian striatum and quenching effects on dopamine-semiquinone generated *in vitro*. Neurol. Res. 27, 533–539.

Asanuma, M., Miyazaki, I., Ogawa, N., 2003. Dopamine- or L-DOPA-induced neurotoxicity: the role of dopamine quinone formation and tyrosinase in a model of Parkinson's disease. Neurotox. Res. 5, 165–176.

Basma, A.N., Morris, E.J., Nicklas, W.J., Geller, H.M., 1995. L-dopa cytotoxicity to PC12 cells in culture is via its autoxidation. J. Neurochem. 64, 825–832.

Chae, S.W., Bang, Y.J., Kim, K.M., Lee, K.Y., Kang, B.Y., Kim, E.M., Inoue, H., Hwang, O., Choi, H.J., 2007. Role of cyclooxygenase-2 in tetrahydrobiopterin-induced dopamine oxidation. Biochem. Biophys. Res. Commun. 359, 735–741.

Choi, H.J., Kim, S.W., Lee, S.Y., Hwang, O., 2003. Dopamine-dependent cytotoxicity of tetrahydrobiopterin: a possible mechanism for selective neurodegeneration in Parkinson's disease. J. Neurochem. 86, 143–152.

Choi, H.J., Lee, S.Y., Cho, Y., Hwang, O., 2005. Inhibition of vesicular monoamine transporter enhances vulnerability of dopaminergic cells: relevance to Parkinson's disease. Neurochem. Int. 46, 329–335.

Foppoli, C., Coccia, R., Cini, C., Rosei, M.A., 1997. Catecholamines oxidation by xanthine oxidase. Biochim. Biophys. Acta 1334, 200–206.

Fornstedt, B., Rosengren, E., Carlsson, A., 1986. Occurrence and distribution of 5-*S*-cysteinyl derivatives of dopamine, dopa and dopac in the brains of eight mammalian species. Neuropharmacology 25, 451–454.

Gerlach, M., Double, K.L., Ben-Shachar, D., Zecca, L., Youdim, M.B., Riederer, P., 2003. Neuromelanin and its interaction with iron as a potential risk factor for dopaminergic neurodegeneration underlying Parkinson's disease. Neurotox. Res. 5, 35–44.

Graham, D.G., 1978. Oxidative pathways for catecholamines in the genesis of neuromelanin and cytotoxic quinones. Mol. Pharmacol. 14, 633–643.

Haque, M.E., Asanuma, M., Higashi, Y., Miyazaki, I., Tanaka, K., Ogawa, N., 2003. Apoptosis-inducing neurotoxicity of dopamine and its metabolites via reactive quinone generation in neuroblastoma cells. Biochim. Biophys. Acta 1619, 39–52.

Hastings, T.G., 1995. Enzymatic oxidation of dopamine: the role of prostaglandin H synthase. J. Neurochem. 64, 919–924.

Hastings, T.G., Lewis, D.A., Zigmond, M.J., 1996. Role of oxidation in the neurotoxic effects of intrastriatal dopamine injections. Proc. Natl. Acad. Sci. U.S.A. 93, 1956–1961.

Kito, M., Maehara, M., Watanabe, K., 1996. Mechanisms of T-type calcium channel blockade by zonisamide. Seizure 5, 115–119.

Komatsu, M., Hiramatsu, M., Willmore, L.J., 2000. Zonisamide reduces the increase in 8-hydroxy-2'-deoxyguanosine levels formed during iron-induced epileptogenesis in the brains of rats. Epilepsia 41, 1091–1094.

Korytowski, W., Sarna, T., Kalyanaraman, B., Sealy, R.C., 1987. Tyrosinase-catalyzed oxidation of dopa and related catechol(amine)s: a kinetic electron spin resonance investigation using spin-stabilization and spin label oximetry. Biochim. Biophys. Acta 924, 383–392.

Kuhn, D.M., Arthur Jr., R.E., Thomas, D.M., Elferink, L.A., 1999. Tyrosine hydroxylase is inactivated by catechol-quinones and converted to a redox-cycling quinoprotein: possible relevance to Parkinson's disease. J. Neurochem. 73, 1309–1317.

Lai, C.T., Yu, P.H., 1997. Dopamine- and L-β-3,4-dihydroxyphenylalanine hydrochloride (L-Dopa)-induced cytotoxicity towards catecholaminergic neuroblastoma SH-SY5Y cells. Effects of oxidative stress and antioxidative factors. Biochem. Pharmacol. 53, 363–372.

LaVoie, M.J., Ostaszewski, B.L., Weihofen, A., Schlossmacher, M.G., Selkoe, D.J., 2005. Dopamine covalently modifies and functionally inactivates parkin. Nat. Med. 11, 1214–1221.

Machida, Y., Chiba, T., Takayanagi, A., Tanaka, Y., Asanuma, M., Ogawa, N., Koyama, A., Iwatsubo, T., Ito, S., Jansen, P.H., Shimizu, N., Tanaka, K., Mizuno, Y., Hattori, N., 2005. Common anti-apoptotic roles of parkin and alpha-synuclein in human dopaminergic cells. Biochem. Biophys. Res. Commun. 332, 233–240.

Miyazaki, I., Asanuma, M., Diaz-Corrales, F.J., Fukuda, M., Kitaichi, K., Miyoshi, K., Ogawa, N., 2006. Methamphetamine-induced dopaminergic neurotoxicity is regulated by quinone formation-related molecules. FASEB J. 20, 571–573.

Miyazaki, I., Asanuma, M., Diaz-Corrales, F.J., Miyoshi, K., Ogawa, N., 2005. Dopamine agonist pergolide prevents levodopa-induced quinoprotein formation in parkinsonian striatum and shows quenching effects on dopamine-semiquinone generated *in vitro*. Clin. Neuropharmacol. 28, 155–160.

Mori, A., Noda, Y., Packer, L., 1998. The anticonvulsant zonisamide scavenges free radicals. Epilepsy Res. 30, 153–158.

Murata, M., 2004. Novel therapeutic effects of the anti-convulsant, zonisamide, on Parkinson's disease. Curr. Pharm. Des. 10, 687–693.

Murata, M., et al., 2007. Zonisamide improves motor function in Parkinson disease: a randomized, double-blind study. Neurology 68, 45–50.

Murata, M., Horiuchi, E., Kanazawa, I., 2001. Zonisamide has beneficial effects on Parkinson's disease patients. Neurosci. Res. 41, 397–399.

Offen, D., Ziv, I., Sternin, H., Melamed, E., Hochman, A., 1996. Prevention of dopamine-induced cell death by thiol antioxidants: possible implications for treatment of Parkinson's disease. Exp. Neurol. 141, 32–39.

Ogawa, N., Asanuma, M., Miyazaki, I., Diaz-Corrales, F.J., Miyoshi, K., 2005. L-DOPA treatment from the viewpoint of neuroprotection: possible mechanism of specific and progressive dopaminergic neuronal death in Parkinson's disease. J. Neurol. 252 (Suppl. 4), iv23–iv31.

Ogawa, N., Edamatsu, R., Mizukawa, K., Asanuma, M., Kohno, M., Mori, A., 1993. Degeneration of dopaminergic neurons and free radicals. Possible participation of levodopa. Adv. Neurol. 60, 242–250.

Ogawa, N., Tanaka, K., Asanuma, M., 2000. Bromocriptine markedly suppress levodopa-induced abnormal increase of dopamine turnover in the parkinsonian striatum. Neurochem. Res. 25, 755–758.

Okada, M., Kaneko, S., Hirano, T., Ishida, M., Kondo, T., Otani, K., Fukushima, Y., 1992. Effects of zonisamide on extracellular levels of monoamine and its metabolite, and on Ca^{2+} dependent dopamine release. Epilepsy Res. 13, 113–119.

Okada, M., Kaneko, S., Hirano, T., Mizuno, K., Kondo, T., Otani, K., Fukushima, Y., 1995. Effects of zonisamide on dopaminergic system. Epilepsy Res. 22, 193–205.

Paz, M.A., Fluckiger, R., Boak, A., Kagan, H.M., Gallop, P.M., 1991. Specific detection of quinoproteins by redox-cycling staining. J. Biol. Chem. 266, 689–692.

Rosei, M.A., Blarzino, C., Foppoli, C., Mosca, L., Coccia, R., 1994. Lipoxygenase-catalyzed oxidation of catecholamines. Biochem. Biophys. Res. Commun. 200, 344–350.

Sulzer, D., Bogulavsky, J., Larsen, K.E., Behr, G., Karatekin, E., Kleinman, M.H., Turro, N., Krantz, D., Edwards, R.H., Greene, L.A., Zecca, L., 2000. Neuromelanin biosynthesis is driven by excess cytosolic catecholamines not accumulated by synaptic vesicles. Proc. Natl. Acad. Sci. U.S.A. 97, 11869–11874.

Sulzer, D., Zecca, L., 2000. Intraneuronal dopamine-quinone synthesis: a review. Neurotox. Res. 1, 181–195.

Suzuki, S., Kawakami, K., Nishimura, S., Watanabe, Y., Yagi, K., Seino, M., Miyamoto, K., 1992. Zonisamide blocks T-type calcium channel in cultured neurons of rat cerebral cortex. Epilepsy Res. 12, 21–27.

Tse, D.C., McCreery, R.L., Adams, R.N., 1976. Potential oxidative pathways of brain catecholamines. J. Med. Chem. 19, 37–40.

Walkinshaw, G., Waters, C.M., 1995. Induction of apoptosis in catecholaminergic PC12 cells by L-DOPA. Implications for the treatment of Parkinson's disease. J. Clin. Invest. 95, 2458–2464.

Whitehead, R.E., Ferrer, J.V., Javitch, J.A., Justice, J.B., 2001. Reaction of oxidized dopamine with endogenous cysteine residues in the human dopamine transporter. J. Neurochem. 76, 1242–1251.

Xu, Y., Stokes, A.H., Roskoski Jr., R., Vrana, K.E., 1998. Dopamine, in the presence of tyrosinase, covalently modifies and inactivates tyrosine hydroxylase. J. Neurosci. Res. 54, 691–697.

Zecca, L., Zucca, F.A., Wilms, H., Sulzer, D., 2003. Neuromelanin of the substantia nigra: a neuronal black hole with protective and toxic characteristics. Trends Neurosci. 26, 578–580.

Magn Reson Med Sci, Vol. 7, No. 3, pp. 163-167, 2008

CASE REPORT

Diffusion Tensor Imaging in Familial Spastic Paraplegia with Mental Impairment and Thin Corpus Callosum

Miho OTA[1], Noriko SATO[1]*, Yuji SAITOH[2], Fumito ENDO[2], Miho MURATA[2], and Takashi ASADA[3]

Departments of [1]Radiology and [2]Neurology, National Center Hospital for Mental, Nervous and Muscular Disorders, National Center of Neurology and Psychiatry
4-1-1, Ogawahigashi, Kodaira, Tokyo 187-8551, Japan
[3]Department of Neuropsychiatry, Institute of Clinical Medicine, University of Tsukuba
(Received April 17, 2008; Accepted July 2, 2008)

We investigated 2 Japanese siblings with a complicated form of familial spastic paraplegia. Cranial magnetic resonance (MR) imaging revealed marked thinning of the corpus callosum. Diffusion tensor imaging (DTI) showed microstructural changes in the thalamus, basal ganglia, and cerebral white matter, and single photon emission computed tomography (SPECT) using 99mTc-ethylcysteinate dimer showed very similar findings. DTI and SPECT effectively revealed global changes not revealed by conventional MR imaging.

Keywords: ***diffusion tensor imaging, familial spastic paraplegia, fractional anisotropy, mean diffusivity***

Introduction

Familial spastic paraplegia (FSP) is clinically and genetically heterogenous. It has been clinically classified into 2 categories, pure spastic paraplegia (pure FSP) and a "complicated" form.[1] In addition to spastic paraplegia, complicated FSP is associated with various somatic abnormalities and neurological deficits, including optic neuropathy, retinopathy, pyramidal symptom, neural amyotrophy, mental impairment, and cerebellar deficit.[1,2]

We report 2 patients with complicated FSP whose unique complications include mental deterioration and thin corpus callosum (CC) on magnetic resonance (MR) imaging. We examined diffusion tensor imaging (DTI) studies of the 2 patients with FSP and normal controls. We also performed single photon emission computed tomography (SPECT) using 99mTc-ethylcysteinate dimer (99mTc-ECD) on the patients.

Case Report

We examined 2 brothers (Patient 1, aged 27 years; Patient 2, 17 years) in a Japanese nuclear family, both of whom were clearly affected by familial spastic paraplegia (FSP) and were admitted to our hospital with progressive gait disturbance that began in their teens and became spastic. Psychomotor development was almost normal. Neurological examination revealed pyramidal signs in the upper and lower limbs in Patient 1 and limited to the lower limbs in Patient 2. No cataracts, retinal degeneration, or cerebellar dysfunction were evident. Patient 1 showed amyotrophy of the upper and lower limbs and trunk, loss of vibratory sensation in the lower limbs, and bladder dysfunction. Patient 2 only exhibited weakness in his lower legs. Evaluation using the Wechsler Adult Intelligence Scale-Revised demonstrated intellectual decline (intelligence quotient [IQ]: Patient 1, 41; Patient 2, 64). Serum vitamin B_{12}, thyroid function, and plasma very-long-chain fatty acid levels were normal. Serum was negative for antihuman T-cell lymphotrophic virus type-1 antibody.

Their father exhibited gait disturbance during his teens but showed no other neurological disturbance or mental deterioration. Their mother was free from degenerative neurological disorders. No other family member of the patients' or their parents' generation appeared to be affected by FSP.

The 2 siblings and 8 normal male controls (mean age = 27.8 ± 1.0 year) underwent magnetic resonance (MR) imaging; only the 2 siblings underwent single photon emission computed tomography

*Corresponding author, Phone: +81-42-341-2711, Fax: +81-42-346-2094, E-mail: snoriko@ncnp.go.jp

(SPECT). We explained the nature and purpose of the diffusion tensor imaging (DTI), MR imaging, and SPECT examinations and received the patients' informed consent. The protocol was approved by the local ethics committee. A complete description of our method was reported previously.[3,4] We performed MR imaging using a 1.0T unit (Magnetom Harmony; Siemens, Erlangen, Germany) with a head coil. Three-dimensional (3D) T_1-weighted images were scanned in the sagittal plane (repetition time/echo time [TR/TE], 2080/3.93 ms; flip angle, 15°; effective section thickness, 1.23 mm; slab thickness, 177 mm; matrix, 208×256; field of view [FOV], 256×315 mm; number of signals acquired, 1), yielding 144 contiguous slices through the head. In addition to 3D T_1-weighted images, we acquired conventional axial T_2-weighted turbo spin echo images (6580/89; slice thickness, 5 mm; intersection gap, 0.4 mm; matrix, 512×532; field of view, 230×230 mm; number of signals acquired, 1). DTI was performed in the axial plane (TE, 113 ms; TR, 10,100 ms; FOV, 230×230 mm^2; matrix, 128×128; 40 continuous transverse slices; slice thickness 3 mm with no intersection gap). To enhance signal-to-noise ratio, we repeated acquisition 5 times. We measured diffusion along 12 noncollinear directions using a diffusion-weighted b factor in each direction of 700 s/mm^2, and we acquired one image without using a diffusion gradient. We performed SPECT of the brain using 3-head rotation gamma cameras (MultiSPECT3; Siemens Medical System, Inc., Hoffman Estate, IL) equipped with high-resolution fan-beam collimators with 600 MBq of 99mTc-ECD. For each camera, projection data were obtained in a 128×128 format for 24 angles at 50 s per angle. A Shepp and Logan Hanning filter was used for SPECT image reconstruction at 0.7 cycle/cm. Attenuation correction was performed using Chang's method.

In Patient 1, T_1- and T_2-weighted cranial MR imaging showed extreme thinning of the CC and atrophy of the frontal, temporal, and parietal cortices (Fig. 1A, B, C). T_2-weighted images showed subtle high intensity in the frontal and parietal white matter (Fig. 1C). In Patient 2, images showed only severe thinning of the CC (Fig. 2A), particularly in the anterior half. No atrophy or abnormal signals were indicated in the cerebral hemispheres, cerebellum, or brainstem, with the exception of mild enlargement of the left trigone of the lateral ventricle (Fig. 2A, B, C). We investigated the regional callosal size, genu, splenium, and body. The corpus callosum was manually traced on the midsagittal slice of the T_1- weighted MR image. In Patient 1, the size of the genu was 28.7 mm^2; body, 86.2 mm^2; and splenium, 43.9 mm^2, In Patient 2, the size of the genu was 16.6 mm^2; body, 99.9 mm^2; and splenium, 96.8 mm^2. In controls, the mean sizes were: genu, 153.9±19.0 mm^2; body, 318.8±39.5 mm^2; and splenium, 83.1±30.3 mm^2.

In Patient 1, 99mTc-ECD SPECT images showed diffuse decrease of blood flow in the cerebral cortex as well as both thalami and the left putamen (Fig. 1D). In Patient 2, SPECT images showed hypoperfusion in the left occipital cortex, both frontal cortices and thalami, and the left striatum (Fig. 2D).

We used the normalization method to investigate the differences of DTI metrics between the patients with FSP and healthy subjects. At normalization, the individual 3D T_1 image was first aligned to its $b=0$ image using statistical parametric mapping (SPM2) (Wellcome Department of Imaging Neuroscience, London, UK), and the aligned T_1 image was normalized to the standard Montreal Neurological Institute space, then the transformation matrix was applied to the fractional anisotropy (FA) and mean diffusivity (MD). Further, to avoid the effect of cerebrospinal fluid (CSF) diffusivity, FA and MD map images were masked with the CSF image derived from the segmented 3D T_1 image using SPM2. Then, each map was spatially smoothed by 5-mm full-width at half the maximum Gaussian. Statistical analyses were performed using SPM2 software. Decrease of FA and increase of MD in the cerebrums of patients with FSP compared to controls were evaluated using 2-sample T-test. Only differences meeting these criteria were deemed statistically significant. In this case, a seed level of $P<0.001$ (uncorrected) and a cluster level of $P<0.05$ (uncorrected) were selected.

The FA and MD values showed significant differences between patients and controls (FA; Figs. 1 E-H and 2 E-H; MD: Figs. 1 I-L and 2 I-L). The DTI metrics, especially the MD values of patients were significantly changed in the thalamus, basal nuclei except for the caudate, and almost entire cerebral white matter in Patient 1. In Patient 2, the decrease of FA value was not obviously detected in thalami and basal nuclei, but MD values were clearly increased as in Patient 1.

Discussion

Complicated FSP is associated with slowly progressive spastic paraplegia of juvenile onset, probably autosomal recessive type inheritance, moderate-to-severe mental impairment, and often, markedly thin corpus callosum. Our patients had quite analogous manifestations and presented similar

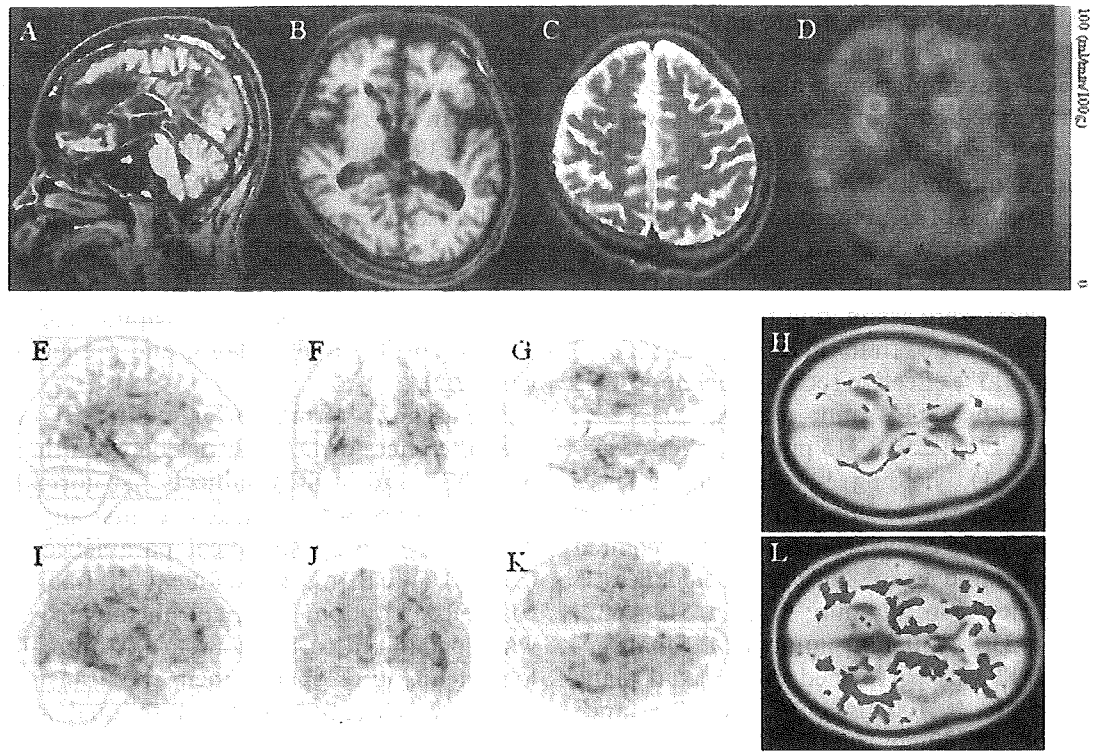

Fig. 1. Patient 1, a 27-year-old man with familial spastic paraplegia. **A**: Sagittal T_1-weighted image shows extremely thin corpus callosum (CC). **B**: Axial T_1-weighted magnetic resonance (MR) image shows frontal, temporal cortical atrophy. The trigones of the lateral ventricle are dilated. **C**: Axial T_2-weighted MR image shows subtle high intensity in the atrophic frontal and parietal white matter. **D**: Single photon emission computed tomography (SPECT) image shows diffuse decrease in blood flow in the cerebral cortex as well as both thalami and the left putamen. **E-H**: The decreased region of fractional anisotropy (FA) value depicted on the standard normalized space (2-sample t-test, statistical parametric mapping [SPM] 2). Significantly low FA values were detected in the thalamus and almost the entire cerebral white matter. **I-L**: The increased region of mean diffusivity (MD) value is shown. Similar to FA study, significantly high MD is revealed.

imaging findings to those of previously reported patients with FSP.[5-7] CC thinning, a characteristic finding, could have resulted from atrophy or hypoplasia.[5-9] However, Nakamura showed that CC thickness did not correlate with duration from onset, and they showed no change on MR imaging in a 5-year follow-up study.[6] Hence, hypoplasia appears the most likely mechanism of CC thinning. Although previous studies discussed causality of hypoplasia, little is known about its origin.[6,7]

Both patients showed global degeneration of white matter. In particular, degeneration of the thalami has been thought to contribute to intellectual decline in patients with FSP,[7] and our results showed high MD in the thalami in both patients, findings consistent with previous postmortem and neuroimaging study.[5,7,9,10] There are thalamic regions with only weak or diffuse cortical connections. Some connections obscured the directionality of diffusion, and the FA map detected no thalamic changes. Additionally, the statistical power of FA was relatively low. Because spatial normalization of subcortical white matter is less effective,[11] the more heterogeneous FA map rather than the relatively uniform MD map cannot be normalized well.[12] So, we could not reveal global white matter change so clearly from statistics using FA than using MD in this study. We could not detect the changes in the CC by DTI analysis but obtained other parts of cerebral FA and MD maps in patients with FSP. Because the abnormal thin structural change of CC and widened lateral cerebral ventricles in patients with FSP influenced the SPM segmentation of 3D-T_1 images, the masking process of the DTI map was ineffective.

DTI revealed diffuse microstructural changes of the white matter not detected by conventional MR imaging. In Patient 2, these changes preceded cortical change. The changes in regional cerebral blood flow revealed by 99mTc-ECD SPECT also preced-

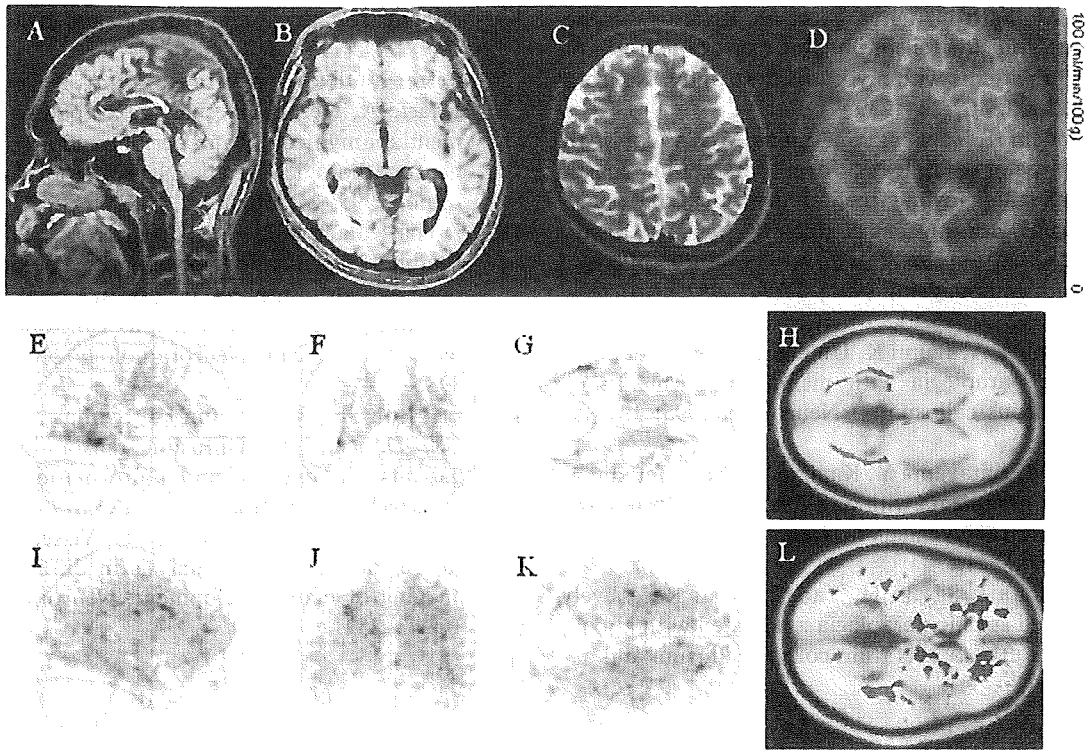

Fig. 2. Patient 2, 17-year-old younger brother with familial spastic paraplegia. **A**: Sagittal T_1-weighted image showing thin corpus callosum (CC), particularly in the anterior half. **B**: Axial T_1-weighted MR image shows relatively preserved cortex. The trigone of the left lateral ventricle is slightly dilated. **C**: Axial T_2-weighted magnetic resonance (MR) image shows no abnormal signals. **D**: Single photon emission computed tomography (SPECT) image shows hypoperfusion in the left occipital cortex, both frontal cortices and thalami, and the left striatum. **E-H**: The decreased region of fractional anisotropy (FA) value depicted on the standard normalized space (2-sample t-test, statistical parametric mapping [SPM] 2). Significantly low FA value was detected in the entire cerebral white matter, especially the optic radiations. **I-L**: The increased region of MD value is shown. Significantly high MD was revealed, similar to the findings in Patient 1.

ed structural changes measured by conventional MR imaging. The present SPECT findings showed relative preservation of the caudate blood flow, which was consistent with DTI findings. Previous study investigating FSP using MR spectroscopy and DTI indicated that the primary pathophysiological process in FSP affects the axon, possibly as a result of impaired axonal trafficking.[10] The same pattern of DTI metrics and cerebral blood flow changes reported here may be attributed to this pathophysiological process.

Conclusion

DTI revealed microstructural global changes of the white matter well, and such changes predate cortical deterioration. Changes in regional cerebral blood flow also preceded changes measured by conventional MR imaging, and DTI by MR and SPECT equally showed early pathophysiological process in FSP. Furthermore, DTI does not expose patients to radiation and is cost effective. We therefore recommend noninvasive DTI as equivalent to SPECT for evaluating intracranial morphometric changes in patients affected by FSP.

References

1. Harding AE. Complicated forms of hereditary spastic paraplegia, In: Harding AE, eds. The hereditary ataxias and related disorders. London: Churchill Livingstone, 1984; 191-204.
2. Sutherland JM. Familial spastic paraplegia, In: Vinken PJ, Bruyn GW, eds. Handbook of clinical neurology, vol. 22. Amsterdam: North-Holland, 1975; 421-431.
3. Hirao K, Ohnishi T, Hirata Y, et al. The prediction of rapid conversion to Alzheimer's disease in mild cognitive impairment using regional cerebral blood flow SPECT. Neuroimage 2005; 28:1014-1021.

4. Ota M, Sato N, Ohya Y, et al. Relationship between diffusion tensor imaging and brain morphology in patients with myotonic dystrophy. Neurosci Lett 2006; 407:234–239.
5. Iwabuchi K, Yagishita S, Amano N, Kosaka K. [A new type of complicated form of hereditary spastic paraplegia showing mental deterioration, quadriplegia with muscular atrophy, sensory disturbance, extrapyramidal disorders, and epilepsy.] Rinsho Shinkeigaku 1991; 31:945–952. Article in Japanese.
6. Nakamura A, Izumi K, Umehara F, et al. Familial spastic paraplegia with mental impairment and thin corpus callosum. J Neurol Sci 1995; 131:35–42.
7. Ueda M, Katayama Y, Kamiya T, et al. Hereditary spastic paraplegia with a thin corpus callosum and thalamic involvement in Japan. Neurology 1998; 51:1751–1754.
8. Yamashita I, Sasaki H, Yabe I, et al. Recessively inherited spastic paraplegia associated with ataxia, congenital cataracts, thin corpus callosum and axonal neuropathy. Acta Neurol Scand 2000; 102:65–69.
9. Ferrer I, Olivé M, Rivera R, Pou A, Narberhaus B, Ugarte A. Hereditary spastic paraparesis with dementia, amyotrophy and peripheral neuropathy. A neuropathological study. Neuropathol Appl Neurobiol 1995; 21:255–261.
10. Dreha-Kulaczewski S, Dechent P, Helms G, Frahm J, Gärtner J, Brockman K. Cerebral metabolic and structural alterations in hereditary spastic paraplegia with thin corpus callosum assessed by MRS and DTI. Neuroradiology 2006; 48:893–898.
11. Eriksson SH, Rugg-Gunn FJ, Symms MR, Barker GJ, Duncan JS. Diffusion tensor imaging in patients with epilepsy and malformations of cortical development. Brain 2001; 124:617–626.
12. Snook L, Plewes C, Beaulieu C. Voxel based versus region of interest analysis in diffusion tensor imaging of neurodevelopment. Neuroimage 2007; 34:243–252.

J Hum Genet (2008) 53:1012–1015
DOI 10.1007/s10038-008-0336-5

SHORT COMMUNICATION

LRRK2 P755L variant in sporadic Parkinson's disease

Hiroyuki Tomiyama · Ikuko Mizuta · Yuanzhe Li · Manabu Funayama · Hiroyo Yoshino · Lin Li · Miho Murata · Mitsutoshi Yamamoto · Shin-ichiro Kubo · Yoshikuni Mizuno · Tatsushi Toda · Nobutaka Hattori

Received: 20 June 2008 / Accepted: 31 August 2008 / Published online: 16 October 2008

Abstract Parkinson's disease (PD) is a neurodegenerative disorder of unknown etiology with probable involvement of genetic-environmental factors. The majority of PD cases (approximately 90–95%) are sporadic, while familial cases account for approximately 5–10% of PD. In a recent report, a heterozygous *LRRK2* P755L mutation within *LRRK2* exon 19 was found in 2% of Chinese sporadic PD patients and in 0% of normal controls or Caucasians, suggesting that the mutation is disease-associated with ethnic specificity. To further evaluate the role of *LRRK2* P755L variant in sporadic PD, we performed direct sequencing of *LRRK2* exon 19 in 501 Japanese sporadic PD patients (male 249, female 252, aged 28–92 years, mean 65.0 years) and 583 controls of the Japanese general population as an extended association study. In this group, we found six patients (6/501 = 1.2%) and eight controls of the general population (8/583 = 1.6%) with a heterozygous P755L variant ($P = 0.80$, $\chi^2 = 0.064$). No other variants were found in exon 19. Together with previous reports, our extended case-controlled study of large sample size suggests that *LRRK2* P755L is a non-disease-associated polymorphism in PD patients.

Keywords Parkinson's disease · Genetics · *PARK8* · *Leucine-rich repeat kinase 2 (LRRK2)* · Polymorphism · Association study · Japanese · Ethnic background

H. Tomiyama · Y. Li · L. Li · S.-i. Kubo · N. Hattori (✉)
Department of Neurology,
Juntendo University School of Medicine,
2-1-1 Hongo, Bunkyo-ku, Tokyo 113-8421, Japan
e-mail: nhattori@med.juntendo.ac.jp

I. Mizuta · T. Toda
Division of Clinical Genetics,
Osaka University Graduate School of Medicine,
Suita, Japan

I. Mizuta · M. Murata · M. Yamamoto · T. Toda · N. Hattori
Core Research for Evolutional Science and Technology (CREST), Japan Science and Technology Agency,
Saitama, Japan

M. Funayama · H. Yoshino · Y. Mizuno
Research Institute for Diseases of Old Age,
Juntendo University School of Medicine, Tokyo, Japan

M. Murata
Department of Neurology, Musashi Hospital,
National Center of Neurology and Psychiatry, Tokyo, Japan

M. Yamamoto
Department of Neurology,
Kagawa Prefectural Central Hospital, Takamatsu, Japan

Introduction

Parkinson's disease (PD, OMIM #168600) is the second most common neurodegenerative disorder next to Alzheimer's disease. The clinical features are characterized by levodopa-responsive parkinsonism, such as rigidity, resting tremor, bradykinesia, and postural instability. Although the cause of PD remains unclear, genetic-environmental interaction is suggested for the development of the disease. One of the autosomal-dominant forms of PD, *PARK8*, was originally mapped from a Japanese Sagamihara family (Funayama et al. 2002) and *LRRK2* (*PARK8*; *leucine-rich repeat kinase 2*, OMIM *609007) was identified as the causative gene for *PARK8*-linked PD (Paisán-Ruíz et al. 2004; Zimprich et al. 2004). Among *LRRK2* mutations, the most common *LRRK2* G2019S mutation in North Africans and Ashkenazi Jews has shown ethnic differences among Caucasian, Japanese, and Chinese (Nichols et al. 2005; Gilks et al. 2005; Lesage et al. 2006; Tomiyama et al.

2006; Tan et al. 2005). On the other hand, *LRRK2* G2385R variant has recently been found the most common genetic risk factor among Chinese and Japanese, but not Caucasians (Di Fonzo et al. 2006; Funayama et al. 2007; Tan et al. 2007; Farrer et al. 2007). Moreover, in a recent report (Wu et al. 2006), a heterozygous *LRRK2* p.P755L (c.2264c > *t*, rs34410987) mutation within *LRRK2* exon 19, corresponding to a predicted ankyrin-repeat-like domain of LRRK2, was found in 2% (12/598) of Chinese sporadic PD and 0% (0/765) of Chinese normal controls, suggesting its association with the disease. However, *LRRK2* P755L was reported as a polymorphism (3% of 92 normal controls) in the dbSNP database of Taiwanese. Thus, to determine the frequency and the role of *LRRK2* P755L in Asian PD, we screened for *LRRK2* exon 19 in Japanese sporadic PD patients.

Subjects and methods

The nucleotide sequences of *LRRK2* exon 19 were determined by direct sequencing in 501 sporadic Japanese PD patients and 583 controls of the Japanese general population (Table 1). All blood samples and clinical information were obtained by the attending neurologists after obtaining informed consent from their patients. The study was approved by the ethics review committees of Juntendo and Osaka Universities. Diagnosis of PD was made by the attending neurologists based on the presence of parkinsonism and good response to anti-PD treatment. Controls of the Japanese general population were evaluated by neurologists to ensure none of them had PD. DNA was prepared using standard methods. They were amplified by polymerase chain reaction (PCR) of exon 19 and sequenced using BigDye Terminator Chemistry and ABI310 and 3130 Genetic Analyzer (Applied Biosystems, Foster City, CA). Sequences of the primers, conditions of PCR, and conditions of sequencing were based on a previous report (Zimprich et al. 2004).

Results

We found 6 patients (6/501 = 1.2%) and 8 controls of the Japanese general population (8/583 = 1.6%) with a heterozygous P755L variant ($P = 0.80$, odds ratio = 1.15, 95% CI: 0.40–3.32, $\chi^2 = 0.064$) in *LRRK2* exon 19 (Table 2). No other variants were found in exon 19.

Discussion

The purpose of the present study was to clarify the role of an ethnic-specific variant in the causative gene for PD. Although PD is considered a heterogeneous disease with genetic-environmental interaction, some cases certainly exhibit a Mendelian-inherited disease or are associated with strong genetic and ethnic background. Indeed, the reported frequency of *LRRK2* G2385R was higher in Asian sporadic PD patients than in controls (Di Fonzo et al. 2006; Funayama et al. 2007; Tan et al. 2007), although this is not the case in Caucasians. Moreover, Wu et al. (2006) in Nanjing, China, recently reported that a heterozygous *LRRK2* P755L mutation was found in 2% (12/598) of Chinese sporadic PD and 0% (0/765) of normal controls, whereas none (0/463) of the Caucasian PD patients had this mutation (Deng et al. 2007), suggesting ethnic differences, like *LRRK2* G2385R. However, our results of large case-controlled study in Japanese revealed that *LRRK2* P755L is a non-disease associated polymorphism. Consistent with our data, this variant was present at similar frequency in Taiwanese PD patients (7/578 = 0.99%) and Taiwanese normal controls (10/339 = 0.97%) (Di Fonzo et al. 2006). Furthermore, the latest report in the Chinese population in Singapore showed the absence of segregation and association of P755L with PD (case 4/204 = 2.0%, control 6/235 = 2.6%, $P = 0.76$) (Tan et al. 2008). These findings might be based on ethnic or native differences in human migration history or human genetics.

We reported previously that the most common *LRRK2* G2019S mutation in Mendelian-inherited and sporadic PD

Table 1 Profile of analyzed samples in this study

Parameter	Patients	Controls of general population
Total sample, *n* (%)	501 (100)	583 (100)
Male, *n* (%)	249 (49.7)	312 (53.5)
Female, *n* (%)	252 (50.3)	271 (46.5)
Age at sampling (years)[a]	65.0 ± 9.6 (28–92)	45.0 ± 17.0 (21–98)
Male[a]	64.3 ± 10.2 (28–92)	43.6 ± 15.0 (22–92)
Female[a]	65.4 ± 9.9 (28–92)	46.8 ± 19.0 (21–98)
Age at onset (years)[a]	58.0 ± 10.5 (20–88)	
Male[a]	57.7 ± 10.9 (20–88)	
Female[a]	58.3 ± 10.1 (25–82)	

[a] Data are mean ± SD (range)

Table 2 Allele frequency of *LRRK2* c. 2264C > T (p. P755L) in Japanese patients with Parkinson's disease and controls of general population

	Genotype, *n* (%)			Allele, *n* (%)			
	C/C	C/T	T/T	C	T	χ^{2a}	OR (95% CI)
Patients (n = 501)	495 (98.8)	6 (1.2)	0 (0)	996 (99.4)	6 (0.6)	0.06	1.15 (0.40–3.32)
Controls of general population (n = 583)	575 (98.6)	8 (1.4)	0 (0)	1,158 (99.3)	8 (0.7)		

[a] Compared with the control

OR odds ratio, *CI* confidence interval

was rare in Asians compared to North Africans or Caucasians (Tomiyama et al. 2006). *LRRK2* variants are reported to spread worldwide with some ethnic differences among each variant, such as R1441G, R1441C, R1441H (exon 31, ROC domain), G2019S, I2020T (exon 41, MAPKKK domain), and G2385R (exon 48, WD40 domain) (Mata et al. 2005). Since *LRRK2* consists of as many as 51 exons, it is important to decide which exon(s) of this gene should be screened first for efficient analysis of mutation in patients with various ethnic backgrounds. In this regard, *LRRK2* exon 41 and 31 are reasonable to be screened first; however, exon 19 is not likely a candidate exon for causative mutation screening in PD. In addition, although MAPKKK and ROC domain are reported to be associated with kinase activity of LRRK2 (Paisán-Ruíz et al. 2004; Zimprich et al. 2004; Smith et al. 2006), the existence and the role of the predicted ankyrin repeat-like domain in LRRK2 have not been established yet.

So far, *LRRK2* P755L as well as G2385R variants have been found in only Chinese, Taiwanese, and Japanese (Asians) with similar frequencies in some Asians, but have not been found in Caucasians. Thus, these variants could occur independently in very ancient Asians with a single founder effect (Farrer et al. 2007). Although the HapMap project has been very successful, the presence of ethnic differences among *LRRK2* variants such as G2019S, R1441G, G2385R, and P755L suggest that further establishment of ethnic-specific or native-specific data is essential for more accurate SNP analyses and genome-wide association studies.

Conclusion

Our extended association study in Japanese with large sample size suggests that *LRRK2* P755L is a non-disease-associated polymorphism in PD patients.

Acknowledgments The authors thank all the participants. The authors also thank Ms. Yuko Nakabayashi and Ms. Yoko Imamichi for the excellent technical assistance. This work was supported by a grant from Core Research for Evolutional Science and Technology (CREST) of the Japan Science and Technology Agency (JST) and by Grants-in-Aid from the Research Committee of CNS Degenerative Diseases, the Ministry of Health, Labor, and Welfare of Japan.

References

Deng H, Le W, Huang M, Xie W, Pan T, Jankovic J (2007) Genetic analysis of LRRK2 P755L variant in Caucasian patients with Parkinson's disease. Neurosci Lett 419:104–107

Di Fonzo A, Wu-Chou YH, Lu CS, van Doeselaar M, Simons EJ, Rohé CF, Chang HC, Chen RS, Weng YH, Vanacore N, Breedveld GJ, Oostra BA, Bonifati V (2006) A common missense variant in the LRRK2 gene, Gly2385Arg, associated with Parkinson's disease risk in Taiwan. Neurogenetics 7:133–138

Farrer MJ, Stone JT, Lin CH, Dächsel JC, Hulihan MM, Haugarvoll K, Ross OA, Wu RM (2007) Lrrk2 G2385R is an ancestral risk factor for Parkinson's disease in Asia. Parkinsonism Relat Disord 13:89–92

Funayama M, Hasegawa K, Kowa H, Saito M, Tsuji S, Obata F (2002) A new locus for Parkinson's disease (PARK8) maps to chromosome 12p11.2–q13.1. Ann Neurol 51:296–301

Funayama M, Li Y, Tomiyama H, Yoshino H, Imamichi Y, Yamamoto M, Murata M, Toda T, Mizuno Y, Hattori N (2007) Leucine-rich repeat kinase 2 G2385R variant is a risk factor for Parkinson disease in Asian population. NeuroReport 18:273–275

Gilks WP, Abou-Sleiman PM, Gandhi S, Jain S, Singleton A, Lees AJ, Shaw K, Bhatia KP, Bonifati V, Quinn NP, Lynch J, Healy DG, Holton JL, Revesz T, Wood NW (2005) A common LRRK2 mutation in idiopathic Parkinson's disease. Lancet 365:415–416

Lesage S, Durr A, Tazir M, Lohmann E, Leutenegger AL, Janin S, Pollak P, Brice A, French Parkinson's Disease Genetics Study Group (2006) LRRK2 G2019S as a cause of Parkinson's disease in North African Arabs. N Engl J Med 354:422–423

Mata IF, Kachergus JM, Taylor JP, Lincoln S, Aasly J, Lynch T, Hulihan MM, Cobb SA, Wu RM, Lu CS, Lahoz C, Wszolek ZK, Farrer MJ (2005) Lrrk2 pathogenic substitutions in Parkinson's disease. Neurogenetics 17:1–7

Nichols WC, Pankratz N, Hernandez D, Paisán-Ruíz C, Jain S, Halter CA, Michaels VE, Reed T, Rudolph A, Shults CW, Singleton A, Foroud T, Parkinson Study Group-PROGENI investigators (2005) Genetic screening for a single common LRRK2 mutation in familial Parkinson's disease. Lancet 365:410–412

Paisán-Ruíz C, Jain S, Evans EW, Gilks WP, Simón J, van der Brug M, López de Munain A, Aparicio S, Gil AM, Khan N, Johnson J, Martinez JR, Nicholl D, Carrera IM, Pena AS, de Silva R, Lees A, Martí-Massó JF, Pérez-Tur J, Wood NW, Singleton AB (2004) Cloning of the gene containing mutations that cause PARK8-linked Parkinson's disease. Neuron 44:595–600

Smith WW, Pei Z, Jiang H, Dawson VL, Dawson TM, Ross CA (2006) Kinase activity of mutant LRRK2 mediates neuronal toxicity. Nat Neurosci 9(10):1231–1233

Tan EK, Shen H, Tan LC, Farrer M, Yew K, Chua E, Jamora RD, Puvan K, Puong KY, Zhao Y, Pavanni R, Wong MC, Yih Y, Skipper L, Liu JJ (2005) The G2019S LRRK2 mutation is uncommon in an Asian cohort of Parkinson's disease patients. Neurosci Lett 384:327–329

Tan EK, Zhao Y, Skipper L, Tan MG, Di Fonzo A, Sun L, Fook-Chong S, Tang S, Chua E, Yuen Y, Tan L, Pavanni R, Wong MC, Kolatkar P, Lu CS, Bonifati V, Liu JJ (2007) The LRRK2 Gly2385Arg variant is associated with Parkinson's disease: genetic and functional evidence. Hum Genet 120:857–863

Tan EK, Lim HQ, Yuen Y, Zhao Y (2008) Pathogenicity of LRRK2 P755L variant in Parkinson's disease. Mov Disord (online 8 Feb 2008)

Tomiyama H, Li Y, Funayama M, Hasegawa K, Yoshino H, Kubo S, Sato K, Hattori T, Lu CS, Inzelberg R, Djaldetti R, Melamed E, Amouri R, Gouider-Khouja N, Hentati F, Hatano Y, Wang M, Imamichi Y, Mizoguchi K, Miyajima H, Obata F, Toda T, Farrer MJ, Mizuno Y, Hattori N (2006) Clinicogenetic study of mutations in *LRRK2* exon 41 in Parkinson's disease patients from 18 countries. Mov Disord 21:1102–1108

Wu T, Zeng Y, Ding X, Li X, Li W, Dong H, Chen S, Zhang X, Ma G, Yao J, Deng X (2006) A novel P755L mutation in LRRK2 gene associated with Parkinson's disease. NeuroReport 17:1859–1862

Zimprich A, Biskup S, Leitner P, Lichtner P, Farrer M, Lincoln S, Kachergus J, Hulihan M, Uitti RJ, Calne DB, Stoessl AJ, Pfeiffer RF, Patenge N, Carbajal IC, Vieregge P, Asmus F, Müller-Myhsok B, Dickson DW, Meitinger T, Strom TM, Wszolek ZK, Gasser T (2004) Mutations in LRRK2 cause autosomal-dominant parkinsonism with pleomorphic pathology. Neuron 44:601–607

Acta Neuropathol (2008) 116:561–566
DOI 10.1007/s00401-008-0425-8

ORIGINAL PAPER

Plaque-type deposition of prion protein in the damaged white matter of sporadic Creutzfeldt-Jakob disease MM1 patients

Atsushi Kobayashi · Kunimasa Arima · Masafumi Ogawa · Miho Murata · Takahiro Fukuda · Tetsuyuki Kitamoto

Received: 29 July 2008 / Revised: 20 August 2008 / Accepted: 20 August 2008 / Published online: 28 August 2008

Abstract Plaque-type deposition of prion protein (PrP) in the brain has been extremely rare in sporadic Creutzfeldt-Jakob disease patients with methionine homozygosity at polymorphic codon 129 of the PrP gene and type 1 abnormal isoform of PrP (sCJD-MM1). Here we report three sCJD-MM1 patients who showed prominent PrP-positive amyloid plaques in the cerebral and cerebellar white matter. All three patients showed clinical courses of long duration (2 years ≤), particularly at the end-stage. The white matter of these patients was severely damaged because of the prolonged disease duration. Furthermore, Alzheimer's amyloid precursor protein, which accumulates within the axonal swellings under pathological conditions, co-accumulated with the PrP-amyloid plaques. These findings suggest that the axonal damage reflecting the prolonged disease duration causes the deposition of PrP-amyloid plaques in the white matter. The present study shows that PrP-amyloid plaques can occur in the white matter of sCJD-MM1 cases.

Keywords Creutzfeldt-Jakob disease · Prion protein · Amyloid plaque · White matter

A. Kobayashi · T. Kitamoto (✉)
Division of CJD Science and Technology,
Department of Prion Research,
Tohoku University Graduate School of Medicine,
2-1 Seiryo-machi, Aoba-ku, Sendai 980-8575, Japan
e-mail: kitamoto@mail.tains.tohoku.ac.jp

K. Arima
Department of Laboratory Medicine,
National Center of Neurology and Psychiatry Musashi Hospital,
4-1-1 Ogawa-higashi-machi, Kodaira 187-8511, Japan

M. Ogawa · M. Murata
Department of Neurology,
National Center of Neurology and Psychiatry Musashi Hospital,
4-1-1 Ogawa-higashi-machi, Kodaira 187-8511, Japan

T. Fukuda
Division of Neuropathology,
Department of Neuroscience, Research Center for Medical Sciences, The Jikei University School of Medicine,
3-25-8 Nishi-Shimbashi, Minato-ku 105-8461, Japan

Introduction

The clinicopathologic phenotypes of sporadic Creutzfeldt-Jakob disease (sCJD) correlate with the genotype [methionine (M) or valine (V)] at polymorphic codon 129 of the prion protein (PrP) gene and the type (type 1 or type 2) of abnormal isoform of PrP (PrP^{Sc}) in the brain [14–16]. Type 1 and type 2 PrP^{Sc} are distinguishable according to the size of the proteinase K-resistant core of PrP^{Sc} (PrP^{res}) (21 and 19 kDa, respectively), reflecting differences in the proteinase K-cleavage site (at residues 82 and 97, respectively) [14, 17]. Based on the genotype and the PrP^{Sc} type, sCJD can be classified into six groups (MM1, MM2, MV1, MV2, VV1 and VV2) [16].

Nearly 70% of sCJD cases are classified as MM1 [16]. sCJD-MM1 is characterized by a clinical course of short duration (mean duration: 3.9 months) and synaptic-type PrP deposition in the brain [16]. However, a small subpopulation of sCJD-MM1 shows long disease duration over several years [16]. The prolonged disease duration might be due to the younger age at onset [18], or to the intensive care of the patients [5], since a comprehensive study revealed no significant difference in the physicochemical properties of PrP^{Sc} between the sCJD-MM1 cases with short and long disease duration[2]. By contrast, the synaptic-type PrP deposition is a common feature of sCJD-MM1 cases. Plaque-type PrP deposition has been extremely rare in sCJD-MM1 cases [16].

Table 1 Summary of the clinical features

	Patient 1	Patient 2	Patient 3
Sex	Male	Male	Female
Age at onset (years)	69	63	71
Initial symptoms	Progressive dementia Fatigue	Progressive dementia	Progressive dementia Fatigue
Myoclonus (months)[a]	5	8	3
Akinetic mutism (months)[a]	7	12[b]	6
PSWC on EEG (months)[a]	5	–[c]	2
Duration (months)	38	24	24

[a] The duration until the appearance of myoclonus, akinetic mutism, or PSWC from onset

[b] The patient became bedridden 7 months after the initial symptoms

[c] Only a single EEG examination was performed 2 months after the initial symptoms. EEG revealed a short burst of delta waves and slowing of background activities

Here we report three sCJD-MM1 patients with prominent PrP-positive amyloid plaques in the cerebral and cerebellar white matter. All three patients showed clinical courses of long duration. Therefore, we discuss correlations among the long disease duration, white matter involvement, and PrP-amyloid plaques.

Patients and methods

Patients

The clinical features of the three patients are summarized in Table 1 and Fig. 1. The clinical signs at onset were complaint of fatigue and progressive dementia (memory loss, disorientation and miscalculation). Electroencephalogram (EEG) showed periodic sharp wave complex (PSWC) in patients 1 and 3. In patient 2, only a single EEG examination was performed 2 months after the initial symptoms, which revealed a short burst of delta waves and slowing of background activities. The patients became bedridden 5 months (patient 1), 7 months (patient 2), or 4 months (patient 3) after the initial symptoms, and then fell into akinetic mutism 7 months (patient 1), 12 months (patient 2), or 6 months (patient 3) after the onset. The total disease duration was 38 months (patient 1) or 24 months (patients 2 and 3). The past medical history was unremarkable with no neurological surgery, no exposure to iatrogenic CJD, and no brain trauma. There was no family history of similar disorders.

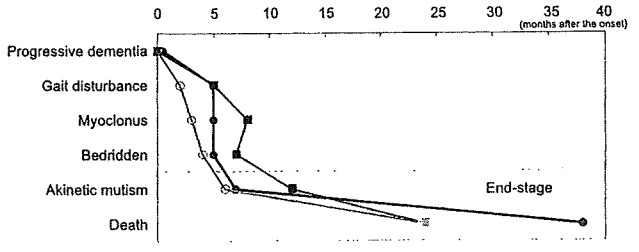

Fig. 1 The clinical courses of patient 1 (*filled circle*), patient 2 (*filled square*), and patient 3 (*open circle*). After the rapid exacerbation period, a prolonged end-stage followed

PrP gene analysis

Genomic DNA was extracted from peripheral blood leukocytes, and the coding region of the PrP gene was analyzed as previously described [7].

Western blot analysis

Brain tissues were obtained at autopsy after receiving informed consent for research use. The brains were immediately frozen or fixed in 10% buffered formalin. PrP^{Sc} was extracted from the frontal cortex with collagenase treatment as described [3] with modifications. Samples were subjected to 13.5% SDS-PAGE and western blotting as described [1]. The 3F4 monoclonal antibody (Signet Laboratories) was used as the primary antibody. Goat-anti-mouse immunoglobulin polyclonal antibody labeled with the peroxidase-conjugated dextran polymer, EnVision+ (DakoCytomation), was used as the secondary antibody.

Neuropathology

Formalin-fixed brains were treated with 99% formic acid for 1 h to inactivate the infectivity and were embedded in paraffin. Tissue sections were stained with hematoxylin and eosin (H&E) for routine neuropathological examination. For Congo red staining, tissue sections were incubated in a solution containing 1% Congo red and 50% ethanol for

30 min. After washing with a solution containing 50% ethanol and 1% sodium hydroxide, the sections were counterstained with hematoxylin. For the PrP immunohistochemistry, tissue sections were pretreated by hydrolytic autoclaving [6]. The #71 monoclonal antibody was used as the primary antibody [10, 19]. Anti-mouse EnVision+ was used as the secondary antibody. For the immunohistochemical detection of the Alzheimer's amyloid precursor protein (APP), tissue sections were pretreated by hydrated autoclaving with 10 mM EDTA pH 6.0 [11, 20]. The UT-18 polyclonal antibody was used as the primary antibody [21]. Anti-rabbit EnVision+ was used as the secondary antibody. The color was developed with diaminobenzidine for single immunostaining or with diaminobenzidine and cobalt chloride [12] for double staining. For double staining with Congo red, the color-developed immunostained sections were washed with water for 5 min and then stained with Congo red as described earlier. In this paper, we term PrP deposits clearly observed on H&E-stained sections and showing green birefringence on adjacent Congo red-stained sections as (amyloid) plaques. Focal PrP-immunolabelings are generically termed as plaque-type PrP deposits, which include amyloid plaques.

Results

PrP gene analysis

All three patients were homozygous for methionine at polymorphic codon 129 (129 M/M) and for glutamic acid at polymorphic codon 219 (219E/E) of the PrP gene. There was no mutation in the coding region of the PrP gene.

Western blot analysis

Western blot analysis of the brains after proteinase-K digestion revealed that the size of PrP^{res} was identical with type 1 PrP^{res} from a typical sCJD-MM1 case (Fig. 2). Type 2 PrP^{res} was not detected.

Neuropathology

The brains weighed 680 g (patient 1), 1,000 g (patient 2), or 840 g (patient 3). The cerebral cortex was very thin, and the white matter was atrophic. On microscopic examination, severe neuronal loss and marked astrocytosis were observed in the cerebral cortex, thalamus and cerebellar cortex (Fig. 3a). The basal ganglia, hippocampus and brainstem were relatively spared. The cerebral and cerebellar white matter showed severe degeneration with the infiltration of macrophages. In patients 1 and 2, many amyloid plaques were observed in the white matter of the

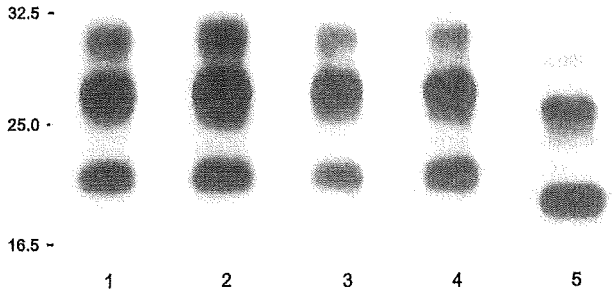

Fig. 2 Western blot analysis of PrP^{res} in the homogenates of the frontal cortex from patient 1 (*lane 2*), patient 2 (*lane 3*), or patient 3 (*lane 4*). The size and glycosylation pattern of PrP^{res} from the three patients were identical with type 1 PrP^{res} from a typical sCJD-MM1 case (*lane 1*), but different from type 2 PrP^{res} from a sCJD-MM2 case (*lane 5*)

cerebral cortex, parahippocampal gyrus, basal ganglia, thalamus, and cerebellar cortex (Fig. 3b). Congo red staining revealed that these amyloid plaques showed green birefringence under polarized light (Fig. 3c). Immunohistochemical analysis using anti-human PrP antibody #71 revealed numerous plaque-type PrP deposits in the white matter besides synaptic-type PrP deposition in the grey matter (Fig. 3d–f). PrP-positive plaques were prominent particularly in the parahipocampal gyrus and basal ganglia (Table 2). In patient 3, plaque-type PrP deposition in the white matter was restricted to within the parahippocampal gyrus.

To evaluate the extent of the axonal damage, we investigated the accumulation of APP in the white matter. APP accumulates within the axonal swellings of brain lesions such as those by infarction [13]. Therefore, we performed immunohistochemical analysis using anti-APP polyclonal antibody UT-18 [21]. In patients 1 and 2, there were many APP immunoreactivities in the white matter of the parahippocamupal gyrus and basal ganglia (Fig. 4a). The accumulation of APP was also observed in the white matter of the frontal and temporal cortex of patient 2. APP accumulation was not observed in the brain sections from patient 3 or typical sCJD-MM1 cases with short disease duration (data not shown). Thus, the intensity and distribution of APP immunoreactivities in the white matter correlated well with those of PrP-amyloid plaques. Furthermore, some of these APP immunoreactivities were enclosed in amyloid plaque-like structures (Fig. 4b). Double staining with APP immunohistochemistry and Congo red revealed the co-localization of APP and amyloid plaques (Fig. 4c). To examine the co-accumulation of APP and PrP, we performed immunohistochemical analysis of the serial sections using anti-APP or anti-PrP antibody. A significant portion of the APP immunoreactivities was co-localized with PrP-amyloid plaques in patients 1 and 2 (Fig. 4d, e).

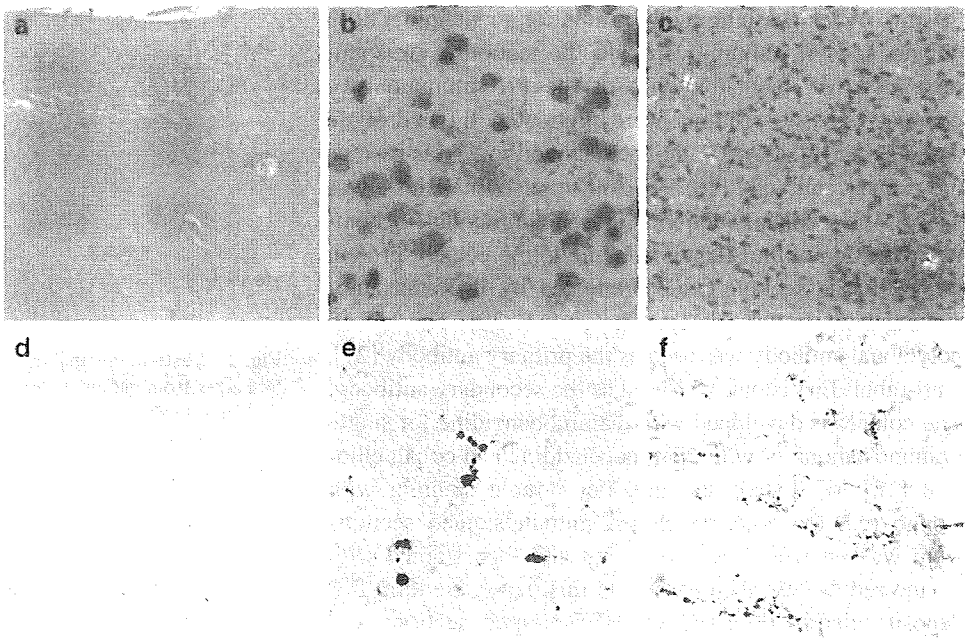

Fig. 3 **a** The cerebral cortex showed extensive neuronal loss and gliosis. The white matter was also severely damaged (frontal cortex of patient 2; H&E; ×20). **b** Amyloid plaque in the basal ganglia (patient 2; H&E; ×600). **c** Amyloid plaques in the white matter were stained with Congo red and showed green birefringence under polarized light (parahippocampal gyrus of patient 1; Congo red; ×200). **d–f** Immunohistochemistry for PrP revealed numerous plaque-type PrP deposits in the white matter of the frontal cortex (**d** patient 2; #71 antibody; ×40), parahippocampal gyrus (**e** patient 1; #71 antibody; ×200), and basal ganglia (**f** patient 2; #71 antibody, ×100)

Table 2 Distribution of PrP-amyloid plaques

Patient	PrP-amyloid plaques in the white matter[a]					
	Frontal cortex	Occipital cortex	Parahippocampus	Basal ganglia	Thalamus	Cerebellum
1	+	–	+++	+++	+	++
2	+++	+	+++	+++	++	++
3	–	–	++	–	–	–

[a] The sum of the number of PrP-positive plaques in 10 fields (×100 magnification)
– 0, + 1–10, ++ 11–100, +++ 100<

Discussion

Here we report three patients with sCJD-MM1 who showed prominent PrP-positive amyloid plaques in the cerebral and cerebellar white matter. PrP-amyloid plaques have been extremely rare in sCJD-MM1 cases, but the present three patients demonstrate that this could occur.

To date, CJD cases with the 129 M/M genotype and plaque-type PrP deposits have been mainly recognized in the infectious form of CJD, e.g., variant CJD (vCJD) or iatrogenic CJD. Only a single sCJD-MM1 case with amyloid plaques has been reported [4], but this case had a history of neurosurgery. Thus, the possibility of iatrogenic transmission of CJD other than sCJD-MM1 could not be excluded. In the present study, however, none of the three patients had any history of neurosurgery or hormone therapy. Moreover, the size of PrP^{res} in the brain was identical with that of type 1 PrP^{res} from a typical sCJD-MM1 case. Type 2 PrP^{res} or the intermediate type PrP^{res} [8], which is observed in vCJD or the plaque-type of dura graft-associated CJD (p-dCJD) cases, was not detected in the brains of the three patients. In addition, PrP-amyloid plaques were restricted within the white matter in the present cases. The distribution of the plaques differed from that observed in vCJD or p-dCJD cases. Therefore, it is certain that the three patients in this report should be classified into sCJD-MM1, but not the infectious form of CJD.

Co-accumulation of APP and PrP suggests that the axonal damage, i.e., impaired axonal transport, causes the deposition of PrP-amyloid plaques in the white matter of sCJD-MM1 cases. APP is transported by the fast anterograde component of axonal flow [9]. Under various pathological conditions, APP accumulates within the axonal swellings because of impaired axonal transport [13]. In the present study, PrP-amyloid plaques were identified exclusively in the white matter and most commonly in conjunction with APP. These findings indicate that PrP might accumulate within the axonal swellings in the damaged white matter and then form amyloid plaques. However, since plaque-type PrP deposits were more than APP deposits in all brain sections examined and APP accumulation was not observed in patient 3, we cannot rule out the reverse hypothesis that PrP-plaques in the white matter induce the axonal damage in case of long disease duration.

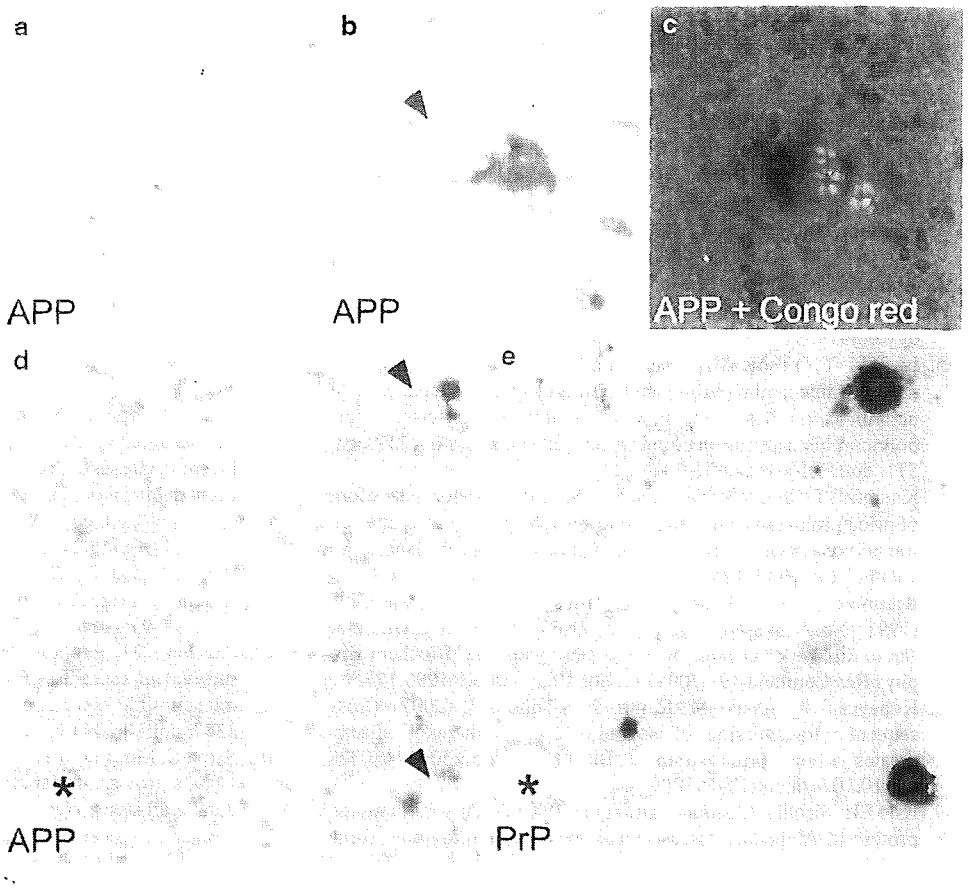

Fig. 4 **a** Immunohistochemistry using anti-APP antibody revealed many APP accumulations in the cerebral white matter (basal ganglia of patient 2; UT-18 antibody; ×100). **b** APP immunoreactivity adjacent to amyloid plaque-like structure (*arrowhead*) (basal ganglia of patient 2, UT-18 antibody; ×600). **c** Double staining with the APP immunohistochemistry and Congo red revealed co-localization of APP and amyloid plaques (basal ganglia of paeitnt 2; UT-18 antibody and Congo red; ×400). **d, e** Immunohistochemical analysis of the serial sections using anti-APP or anti-PrP antibody revealed that the APP immunoreactivities were co-localized with PrP-positive amyloid plaques (*arrowheads*) (parahippocampal gyrus of patient 1; **d** UT-18 antibody; **e** #71 antibody; ×400). *Asterisk* denotes a landmark vessel to indicate the serial sections

The most plausible explanation for the axonal damage is the prolonged disease duration. The three patients in this report showed clinical courses of long duration (2 years ≤). In sCJD-MM1 cases with long disease duration, the white matter is severely affected as the end-stage pathology of CJD [2, 5]. These findings lead us to surmise that PrP-amyloid plaques in the white matter may be a common feature of sCJD-MM1 cases with prolonged disease duration. However, it has been reported that four Japanese sCJD-MM1 cases with long disease duration of over 2 years showed no plaque-type PrP deposition in the white matter [5]. Therefore, not only the disease duration but also unidentified factors such as pharmacological treatment, minor trauma, or hypoxia during the clinical course might modify the pattern of PrP deposition.

As an explanation for PrP-amyloid plaques, we cannot rule out the possible existence of different prion strains in sCJD-MM1 prions. However, the biochemical properties of PrP^{Sc} in the brain are identical between the sCJD-MM1 cases with long and short disease duration [2]. In line with these findings, the three patients in this report had type 1 PrP^{res} identical in size and glycoform ratio to that from typical sCJD-MM1 cases. In addition, in contrast to the prolonged end-stage, the exacerbation periods of the three patients were as short as those of typical sCJD-MM1 cases. Thus, it is highly unlikely that an atypical prion strain caused PrP-amyloid plaques in the present cases. To exclude this possibility, it will be necessary to perform a transmission study using sCJD-MM1 prions from the present three patients.

In conclusion, this study shows that PrP-amyloid plaques can occur in the white matter of sCJD-MM1 cases with prolonged disease duration. Although plaque-type PrP deposition is a characteristic of other subtypes of CJD including sCJD-MV2, VV2, vCJD or p-dCJD, the plaques in the white matter of these cases might also have resulted from the axonal damage reflecting the prolonged disease duration rather than prion strain-dependent properties.

Acknowledgments We thank H. Kudo, K. Abe and M. Kimura for their technical assistance, and B. Bell for critical review of the manuscript. We are grateful to Dr. T. Suzuki for providing the UT-18 antibody. This study was supported by the Program for Promotion of Fundamental Studies in Health Sciences of National Institute of Biomedical Innovation (T.K.), a grant from the Ministry of Health, Labor and Welfare (A.K. and T.K.), and a Grant-in-Aid for Scientific Research from the Ministry of Education, Culture, Sports, Science and Technology (A.K. and T.K.).

References

1. Asano M, Mohri S, Ironside JW, Ito M, Tamaoki N, Kitamoto T (2006) vCJD prion acquires altered virulence through trans-species

infection. Biochem Biophys Res Commun 342:293–299. doi:10.1016/j.bbrc.2006.01.149
2. Cali I, Castellani R, Yuan J et al (2006) Classification of sporadic Creutzfeldt-Jakob disease revisited. Brain 129:2266–2277. doi:10.1093/brain/awl224
3. Grathwohl KUD, Horiuchi M, Ishiguro N, Shinagawa M (1996) Improvement of PrP^{Sc}-detection in mouse spleen early at the preclinical stage of scrapie with collagenase-completed tissue homogenization and Sarkosyl-NaCl extraction of PrP^{Sc}. Arch Virol 141:1863–1874. doi:10.1007/BF01718200
4. Ishida C, Kakishima A, Okino S et al (2003) Sporadic Creutzfeldt-Jakob disease with MM1-type prion protein and plaques. Neurology 60:514–517
5. Iwasaki Y, Yoshida M, Hashizume Y, Kitamoto T, Sobue G (2006) Clinicopathologic characteristics of sporadic Japanese Creutzfeldt-Jakob disease classified according to prion protein gene polymorphism and prion protein type. Acta Neuropathol 112:561–571. doi:10.1007/s00401-006-0111-7
6. Kitamoto T, Shin RW, Doh-ura K et al (1992) Abnormal isoform of prion proteins accumulates in the synaptic structures of the central nervous system in patients with Creutzfeldt-Jakob disease. Am J Pathol 140:1285–1294
7. Kitamoto T, Ohta M, Doh-ura K, Hitoshi S, Terao Y, Tateishi J (1993) Novel missense variants of prion protein in Creutzfeldt-Jakob disease or Gerstmann-Sträussler syndrome. Biochem Biophys Res Commun 191:709–714. doi:10.1006/bbrc.1993.1275
8. Kobayashi A, Asano M, Mohri S, Kitamoto T (2007) Cross-sequence transmission of sporadic Creutzfeldt-Jakob disease creates a new prion strain. J Biol Chem 282:30022–30028. doi:10.1074/jbc.M704597200
9. Koo EH, Sisodia SS, Archer DR et al (1990) Precursor of amyloid protein in Alzheimer disease undergoes fast anterograde axonal transport. Proc Natl Acad Sci USA 87:1561–1565. doi:10.1073/pnas.87.4.1561
10. Muramoto T, Tanaka T, Kitamoto N et al (2000) Analyasis of Gerstmann-Straussler syndrome with 102Leu219Lys using monoclonal antibodies that specifically detect human prion protein with 219Glu. Neurosci Lett 288:179–182. doi:10.1016/S0304-3940(00)01232-5
11. Murayama H, Shin RW, Higuchi J, Shibuya S, Muramoto T, Kitamoto T (1999) Interaction of aluminum with PHFτ in Alzheimer's disease neurofibrillary degeneration evidenced by desferrioxamine-assisted chelating autoclave method. Am J Pathol 155:877–885
12. Ohgami T, Kitamoto T, Shin RW, Kaneko Y, Ogomori K, Tateishi J (1991) Increased senile plaques without microglia in Alzheimer's disease. Acta Neuropathol 81:242–247. doi:10.1007/BF00305864
13. Ohgami T, Kitamoto T, Tateishi J (1992) Alzheimer's amyloid precursor protein accumulates within axonal swellings in human brain lesions. Neurosci Lett 136:75–78. doi:10.1016/0304-3940(92)90651-M
14. Parchi P, Castellani R, Capellari S et al (1996) Molecular basis of phenotypic variability in sporadic Creutzfeldt-Jakob disease. Ann Neurol 39:767–778. doi:10.1002/ana.410390613
15. Parchi P, Capellari S, Chen SG et al (1997) Typing prion isoforms. Nature 386:232–233. doi:10.1038/386232a0
16. Parchi P, Giese A, Capellari S et al (1999) Classification of sporadic Creutzfeldt-Jakob disease based on molecular and phenotypic analysis of 300 subjects. Ann Neurol 46:224–233. doi :10.1002/1531-8249(199908)46:2<224::AID-ANA12>3.0.CO;2-W
17. Parchi P, Zou W, Wang W et al (2000) Genetic influence on the structural variations of the abnormal prion protein. Proc Natl Acad Sci USA 97:10168–10172. doi:10.1073/pnas.97.18.10168
18. Pocchiari M, Puopolo M, Croes EA et al (2004) Predictors of survival in sporadic Creutzfeldt-Jakob disease and other human transmissible spongiform encephalopathies. Brain 127:2348–2359. doi:10.1093/brain/awh249
19. Satoh K, Muramoto T, Tanaka T et al (2003) Association of an 11–12 kDa protease-resistant prion protein fragment with subtypes of dura graft-associated Creutzfeldt-Jakob disease and other prion diseases. J Gen Virol 84:2885–2893. doi:10.1099/vir.0.19236-0
20. Shin RW, Iwaki T, Kitamoto T, Tateishi J (1991) Hydrated autoclave pretreatment enhances tau immunoreactivity in formalin-fixed normal and Alzheimer's disease brain tissues. Lab Invest 64:693–702
21. Tomita S, Ozaki T, Taru H et al (1999) Interaction of a neuron-specific protein containing PDZ domains with Alzheimer's amyloid precursor protein. J Biol Chem 274:2243–2254. doi:10.1074/jbc.274.4.2243

Treatment of neuromyelitis optica: Current debate

Therapeutic Advances in Neurological Disorders
(2008) 1(1) 43–52
DOI: 10.1177/1756285608093978

Tomoko Okamoto, Masafumi Ogawa, Youwei Lin, Miho Murata, Sachiko Miyake and Takashi Yamamura

***Abstract*:** Neuromyelitis optica (NMO) is an inflammatory demyelinating disease that largely affects optic nerves and spinal cord. Recent studies have identified an elevation of serum anti-aquaporin 4 antibody as a hallmark of NMO. Typical cases of NMO significantly differ from multiple sclerosis (MS) in immunological markers, histopathology, and responses to therapy. In fact, plasma exchange may be more efficacious for NMO than MS, whereas interferon-β is recommended for MS but not for NMO. An emerging idea that pathogenesis of NMO may involve an interaction of the newly identified helper T cell subset, Th17, with B cells offers potential targets of therapy.

***Keywords*:** neuromyelitis optica, multiple sclerosis, Th17 cells, anti-aquaporin-4 antibody, interferon-β

Introduction

Neuromyelitis optica (NMO; Devic syndrome) is an inflammatory disease of the central nervous system (CNS) that affects optic nerves and spinal cord [Jacob *et al.* 2007; Matiello *et al.* 2007; Wingerchuk *et al.* 2007]. In older literature, NMO was defined as a disorder that is characterized by development of a single episode of bilateral optic neuritis and transverse myelitis (Table 1). However, recent studies have indicated that presence of serum antibodies against aquaporin 4 (AQP4), a water channel protein, is a hallmark of NMO and could be essential for making the diagnosis. Since anti-AQP4 antibody became recognised as a serological marker of NMO, the clinical picture of NMO has been significantly broadened. Indeed, when the latest criteria [Wingerchuk *et al.* 2006] are used for diagnosis of NMO, a large majority of the NMO patients follow a relapsing clinical course and sometimes develop brain lesions.

Of interest, NMO has been traditionally separated from multiple sclerosis (MS) in western countries, whereas they have been integrated into the category of MS in Japan, by giving a term 'opticospinal MS (OSMS)'. Because not all OSMS exhibit an elevation of anti-AQP4 antibody titer in the sera, and because OSMS may develop brain lesions characteristic of MS [Barkhof *et al.* 1997], it is still debatable as to whether OSMS and NMO may cover an entirely identical disease spectrum or not.

Nowadays, a large proportion of patients with MS are being treated with standard drugs such as interferon-β and glatiramer acetate. It has been reported that interferon-β may also be efficacious for NMO/OSMS based on analysis of a small number of patients [Saida *et al.* 2005]. However, more recent works have emphasized the differences in immunological and pathological features between NMO and conventional MS, which indicates the relevance of distinctive therapeutic strategies for NMO and MS. The aim of this review is to provide up-dated information on the diagnosis and treatment of NMO and also discuss the immunological pathogenesis of NMO with special reference to a critical interaction between B cells and Th17 cells, a newly identified helper T cell subset [Hsu *et al.* 2008].

Diagnosis of NMO: discovery of anti-aquaporin 4 (AQP4) antibody and its impact

In general, the clinical picture of typical NMO is very different from that of conventional MS. Important points for differential diagnosis are as

Correspondence to:
Takashi Yamamura
Department of Neurology, National Center Hospital of Neurology and Psychiatry, Kodaira, Tokyo, Japan
Department of Immunology, National Institute of Neuroscience, National Center of Neurology and Psychiatry, Kodaira, Tokyo, Japan
yamamura@ncnp.go.jp

Tomoko Okamoto
Masafumi Ogawa
Youwei Lin
Miho Murata
Department of Neurology, Musashi Hospital, National Center of Neurology and Psychiatry, Kodaira, Tokyo, Japan

Youwei Lin
Sachiko Miyake
Department of Immunology, National Institute of Neuroscience, National Center of Neurology and Psychiatry, Kodaira, Tokyo, Japan